Journal of the Mechanics and Physics of Solids 60 (2012) 1907–1921

Contents lists available at SciVerse ScienceDirect

Journal of the Mechanics and Physics of Solids

journal homepage: www.elsevier.com/locate/jmps

Chiral effect in plane isotropic micropolar elasticity and its application to chiral lattices

X.N. Liu [a,b], G.L. Huang [b,*], G.K. Hu [a,*]

[a] Key Laboratory of Dynamics and Control of Flight Vehicle, Ministry of Education, School of Aerospace Engineering, Beijing Institute of Technology, Beijing 100081, China

[b] Department of Systems Engineering, University of Arkansas at Little Rock, Little Rock, Arkansas 72204, United States

ARTICLE INFO

Article history:
Received 30 December 2011
Received in revised form
17 June 2012
Accepted 26 June 2012
Available online 4 July 2012

Keywords:
Chiral micropolar elasticity
Chiral lattice
Constitutive equation
Plane problem

ABSTRACT

In continuum mechanics, the non-centrosymmetric micropolar theory is usually used to capture the chirality inherent in materials. However, when reduced to a two dimensional (2D) isotropic problem, the resulting model becomes non-chiral. Therefore, influence of the chiral effect cannot be properly characterized by existing theories for 2D chiral solids. To circumvent this difficulty, based on reinterpretation of isotropic tensors in the 2D case, we propose a continuum theory to model the chiral effect for 2D isotropic chiral solids. A single material parameter related to chirality is introduced to characterize the coupling between the bulk deformation and the internal rotation, which is a fundamental feature of 2D chiral solids. Coherently, the proposed continuum theory is applied for the homogenization of a triangular chiral lattice, from which the effective material constants of the lattice are analytically determined. The unique behavior in the chiral lattice is demonstrated through the analyses of a static tension problem and a plane wave propagation problem. The results, which cannot be predicted by the non-chiral model, are verified by the exact solution of the discrete model.

1. Introduction

An object is said to be chiral, or with handedness, if it cannot be superposed to its mirror image (Kelvin, 1904). Chirality is encountered in many branches of science, including physics, biology, chemistry and optics. A chiral material should be described by an adequate constitutive equation with handedness in order to characterize the distinct feature of such material. In continuum mechanics, chirality is considered in the context of generalized elasticity, e.g. micropolar (Cosserat) theory (Cosserat and Cosserat, 1909; Eringen, 1966). A general isotropic chiral (also known as non-centrosymmetric, acentric or hemitropic) micropolar theory introduces three additional material constants compared to the non-chiral theory to represent the effect of chirality (Nowacki, 1986; Lakes and Benedict, 1982; Lakes, 2001; Natroshvili and Stratis, 2006; Natroshvili et al., 2006; Joumaa and Ostoja-Starzewski, 2011). The additional material parameters change their signs according to the handedness of the microstructure. This theory provides an efficient tool for modeling the chiral effect presented in materials and structures, e.g., loading transfer in carbon nanotubes and chiral rods (Chandraseker and Mukherjee, 2006; Chandraseker et al., 2009; Ieşan, 2010), mechanics of bone (Lakes et al., 1983), chirality transfer in

* Corresponding authors.
E-mail addresses: glhuang@ualr.edu (G.L. Huang), hugeng@bit.edu.cn (G.K. Hu).

0022-5096/$ - see front matter © 2012 Elsevier Ltd. All rights reserved.
http://dx.doi.org/10.1016/j.jmps.2012.06.008

nanomaterials (Wang et al., 2011) and wave propagation in chiral solids (Lakhtakia et al., 1988; Ro, 1999; Khurana and Tomar, 2009). However, when this theory is applied to a planar isotropic case, e.g. a triangular chiral lattice, the variables describing the chiral effect disappear and the resulting theory becomes basically non-chiral (Spadoni and Ruzzene, 2012). Therefore the basic characteristic of a planar chiral solid cannot be properly modeled by the existing micropolar theory. Recently, the chiral-dependent behavior of planar solids is characterized in the context of strain gradient theory by introducing the high-order elasticity properties (Auffray et al., 2010).

On the other hand, lattice structures can be homogenized as micropolar continuum media (Bazant and Christensen, 1972; Chen et al., 1998; Kumar and McDowell, 2004), the homogenized material constants are derived directly from their microstructures. This provides a useful tool to explain the observed size effect in lattice structures. Chiral lattice structure was also proposed by Prall and Lakes (1996) to achieve a material with negative Poisson's ratio (Lakes, 1987). Among the candidates of these so-called auxetic materials (Yang et al., 2004), the triangular chiral lattice is the mostly investigated one since it is isotropic and the geometric pattern can be controlled by a single continuously varying topological parameter. Its unique mechanical behavior was examined by many researchers under both static (Alderson et al., 2010; Dirrenberger et al., 2011; Spadoni and Ruzzene, 2012) and dynamic (Spadoni et al., 2009) loading conditions with a number of targeted applications. The chiral material was recently used in designing elastic metamaterials with the negative effective bulk modulus (Liu et al., 2011b). Recently Spadoni and Ruzzene (2012) proposed a self-consistent homogenization scheme for a 2D chiral lattice in the framework of the micropolar theory in order to clarify the indeterminacy of the effective shear modulus (Liu et al., 2011a, 2011b). However, since the non-centrosymmetric isotropic micropolar model becomes non-chiral when applied to a planar problem (Spadoni and Ruzzene, 2012), the developed homogenization method in this framework cannot characterize the chiral effect inherent in the material. Therefore we are encountering a challenging problem: for planar isotropic chiral materials, e.g. triangular chiral lattices, we do not have a solid theory either in continuum formulation or in the homogenization method to characterize the chiral effects.

The objective of the paper is to propose a continuum model to capture the chiral effect in planar isotropic chiral solids, and the corresponding effective material constants will be derived for a planar triangular chiral lattice. Some typical examples are conducted to demonstrate the necessity and consistency of the theory in characterizing the chiral effect. The manuscript is organized as follows: in Section 2, a new constitutive relation for a 2D isotropic chiral solid is proposed based on a continuum formulation. In Section 3, a triangular chiral lattice structure is homogenized in the framework of the proposed theory and the effective material constants are derived. In Section 4, a tension and plane wave propagation problems are examined for a planar chiral lattice by the proposed theory. In Section 5 the main result of this work is concluded.

2. Planar isotropic micropolar model with chirality

Characterization of material chirality is closely related to the concept of pseudo (or axial) tensors, they alternate the sign with a mirror reflecting transformation or the handedness change of the underlying coordinate system, and ordinary (or polar) tensors are not affected by such actions (Borisenko and Tarapov, 1979). Both types of tensors coexist in various elastic formulations, but strain energy density must be independent of handedness.

Classical elasticity theory excludes chirality (Lakes and Benedict, 1982), since in the energy density

$$w=\tfrac{1}{2}\varepsilon_{ij}C_{ijkl}\varepsilon_{kl} \tag{1}$$

the strain ε is an ordinary tensor. To maintain w as an ordinary scalar, the elastic tensor C cannot be pseudo. In this paper, micropolar theory (Eringen, 1999) is considered to include chirality. In the micropolar theory, rotational degree of freedom (DOF) ϕ_i is introduced in addition to the displacement u_i on a material point. The strain and curvature play as deformation measures

$$\varepsilon_{kl}=u_{l,k}+e_{lkm}\phi_m \tag{2a}$$

$$\kappa_{kl}=\phi_{k,l} \tag{2b}$$

and the balance of stress σ_{ji} and couple stress m_{ji} are governed by

$$\sigma_{ji,j}=\rho\partial^2 u_i/\partial t^2 \tag{3a}$$

$$m_{ji,j}+e_{ikl}\sigma_{kl}=j\partial^2\phi_i/\partial t^2 \tag{3b}$$

where e_{ijk} is the Levi-Civita tensor, ρ and j are the density and micro-inertia, respectively. In this paper, the Einstein's summation convention is used and the comma in subscript denotes partial differentiation with respect to spatial coordinates. The strain energy density for a general linear elastic micropolar medium is expressed as a quadratic form in terms of asymmetric strain and curvature tensors

$$w=\tfrac{1}{2}\,\varepsilon_{ij}C_{ijkl}\varepsilon_{kl}+\tfrac{1}{2}\kappa_{ij}D_{ijkl}\kappa_{kl}+\varepsilon_{ij}B_{ijkl}\kappa_{kl} \tag{4}$$

where C, D and B are elastic tensors of rank four. Then the constitutive relation can be derived as

$$\sigma_{ij} = C_{ijkl}\varepsilon_{kl} + B_{ijkl}\phi_{k,l} \tag{5a}$$

$$m_{ij} = B_{ijkl}\varepsilon_{kl} + D_{ijkl}\phi_{k,l} \tag{5b}$$

It should be noted that the microrotation vector ϕ_i and curvature tensor κ_{ij} are pseudo, thus in Eq. (4), B_{ijkl} must be a pseudo tensor and thus represent the chirality. A micropolar solid with $B_{ijkl}\neq 0$ is usually referred as a non-centrosymmetric medium. Let us consider the isotropic case and focus only the chiral part of Eq. (5). A general isotropic tensor of rank four takes the form as

$$B_{ijkl} = B_1\delta_{ij}\delta_{kl} + B_2\delta_{ik}\delta_{jl} + B_3\delta_{il}\delta_{jk} \tag{6}$$

where δ_{jk} is Kronecker delta. The chiral part of Eq. (5) then reads

$$\sigma_{ij} = B_1\delta_{ij}\phi_{k,k} + B_2\phi_{i,j} + B_3\phi_{j,i} \tag{7a}$$

$$m_{ij} = B_1\delta_{ij}\varepsilon_{kk} + B_2\varepsilon_{ij} + B_3\varepsilon_{ji} \tag{7b}$$

A planar micropolar problem in x_1-x_2 plane is defined by $u_3=\phi_1=\phi_2=\partial/\partial x_3=0$, while the non-zero quantities are u_α, ϕ_3, $\phi_{3,\alpha}$, $\varepsilon_{\alpha\beta}$, $\sigma_{\alpha\beta}$ and $m_{\alpha 3}$, respectively, with Greek subscripts ranging from 1 to 2. In the 2D case, it is easy to verify that Eq. (7) is trivial, as a result, chirality represented by the isotropic B_{ijkl} disappears. However, for 2D isotropic chiral solids, e.g., planar triangular chiral lattices, chirality is a basic feature of such structures and should be characterized by a correct constitutive modeling. Therefore there should be something missing in Eqs. (5) and (6) when the theory is reduced to the 2D case.

To circumvent this problem, we first discuss some basic properties of isotropic tensors. The basic forms of isotropic tensors of rank 0, 2 and 3 are just the scalar, Kronecker delta δ_{jk} and Levi-Civita tensor e_{ijk}, respectively. A vector which is a tensor of rank one cannot be isotropic, and e_{ijk} is a pseudo tensor. An isotropic tensor with rank greater than three can be constructed by scalar, δ_{jk} and e_{ijk}, just as Eq. (6) for an isotropic tensor of rank four. However, in the 2D case, the Levi-Civita tensor e_{ijk} is restricted to the form $e_{ijk}\equiv e_{3\alpha\beta}$, which is in-plane isotropic and equivalent to an isotropic tensor of rank two. For the same reason, there is no in-plane third order isotropic tensor in the current 2D situation. The isotropic B tensor also vanishes, since the strain energy density of the 2D case can be rewritten as

$$w = \tfrac{1}{2}\,\varepsilon_{\alpha\beta}C_{\alpha\beta\gamma\rho}\varepsilon_{\gamma\rho} + \tfrac{1}{2}\phi_{3,\alpha}D_{\alpha\beta}\phi_{3,\beta} + \varepsilon_{\alpha\beta}B_{\alpha\beta\gamma}\phi_{3,\gamma} \tag{8}$$

where B reduces to the tensor of rank three and cannot be isotropic except zero. However, with $e_{3\alpha\beta}$ and $\delta_{\alpha\beta}$, we have more choices to construct a 2D isotropic tensor of rank four. In particular, we have

$$\overline{C}_{\alpha\beta\gamma\rho} = \overline{C}_1\delta_{\alpha\beta}\delta_{\gamma\rho} + \overline{C}_2\delta_{\alpha\gamma}\delta_{\beta\rho} + \overline{C}_3\delta_{\alpha\rho}\delta_{\beta\gamma} \tag{9a}$$

$$\tilde{C}_{\alpha\beta\gamma\rho} = \tilde{C}_1\delta_{\alpha\beta}e_{3\gamma\rho} + \tilde{C}_2\delta_{\gamma\rho}e_{3\alpha\beta} + \tilde{C}_3\delta_{\alpha\gamma}e_{3\beta\rho} + \tilde{C}_4\delta_{\beta\rho}e_{3\alpha\gamma} + \tilde{C}_5\delta_{\alpha\rho}e_{3\beta\gamma} + \tilde{C}_6\delta_{\beta\gamma}e_{3\alpha\rho} \tag{9b}$$

$$\hat{C}_{\alpha\beta\gamma\rho} = \hat{C}_1e_{3\alpha\beta}e_{3\gamma\rho} + \hat{C}_2e_{3\alpha\gamma}e_{3\beta\rho} + \hat{C}_3e_{3\alpha\rho}e_{3\beta\gamma} \tag{9c}$$

Eq. (9a) is just the 2D version of Eq. (6). By utilizing the identity $e_{3\alpha\beta}e_{3\gamma\rho}=\delta_{\alpha\gamma}\delta_{\beta\rho}-\delta_{\alpha\rho}\delta_{\beta\gamma}$, Eq. (9c) is found to take the same form as Eq. (9a), this is not surprising since $\hat{C}_{\alpha\beta\gamma\rho}$ is the product of two pseudo tensors, hence it is an ordinary tensor. In summary, we conclude that for a 2D micropolar medium the generic form of an isotropic tensor of rank four can be given as

$$C_{\alpha\beta\gamma\rho} = \overline{C}_{\alpha\beta\gamma\rho} + \tilde{C}_{\alpha\beta\gamma\rho} \tag{10}$$

Reexamining the strain energy density in Eq. (8) with the help of Eq. (10) and $D_{\alpha\beta}=D_1\delta_{\alpha\beta}$, we have

$$w = \tfrac{1}{2}\,\varepsilon_{\alpha\beta}\overline{C}_{\alpha\beta\gamma\rho}\varepsilon_{\gamma\rho} + (\tilde{C}_1+\tilde{C}_2)\varepsilon_{\alpha\alpha}e_{3\gamma\rho}\varepsilon_{\gamma\rho} + \tfrac{1}{2}D_1\phi_{3,\alpha}\delta_{\alpha\beta}\phi_{3,\beta} \tag{11}$$

Introducing the Lame's constant λ, μ, antisymmetric shear modulus κ, higher order modulus γ, and a single chiral parameter $2A\equiv\tilde{C}_1+\tilde{C}_2$, the in-plane isotropic micropolar elastic tensors with chirality are written as

$$\overline{C}_{\alpha\beta\gamma\rho} = \lambda\delta_{\alpha\beta}\delta_{\gamma\rho} + (\mu+\kappa)\delta_{\alpha\gamma}\delta_{\beta\rho} + (\mu-\kappa)\delta_{\alpha\rho}\delta_{\beta\gamma} \tag{12a}$$

$$\tilde{C}_{\alpha\beta\gamma\rho} = A(\delta_{\alpha\beta}e_{3\gamma\rho} + \delta_{\gamma\rho}e_{3\alpha\beta}), \tag{12b}$$

$$\overline{D}_{\alpha\beta} = \gamma\delta_{\alpha\beta} \tag{12c}$$

Note that Eq. (12b) has a symmetric form with the requirement of major symmetry for the C tensor. The constitutive equation then becomes

$$\sigma_{\alpha\beta} = \lambda\delta_{\alpha\beta}\varepsilon_{\rho\rho} + (\mu+\kappa)\varepsilon_{\alpha\beta} + (\mu-\kappa)\varepsilon_{\beta\alpha} + A\delta_{\alpha\beta}e_{3\gamma\rho}\varepsilon_{\gamma\rho} + Ae_{3\alpha\beta}\varepsilon_{\rho\rho} \tag{13}$$

$$m_{\alpha 3} = \gamma\phi_{3,\alpha}$$

It is interesting to note that the pseudo tensor $\tilde{C}_{\alpha\beta\gamma\rho}$ representing the chirality relates to both the normal stress and normal strain, this is different from the B_{ijkl} tensor in the 3D case. However, the physical meaning of $\tilde{C}_{\alpha\beta\gamma\rho}$ is very clear. Consider the relevant part in Eq. (11)

$$A(\delta_{\alpha\beta}e_{3\gamma\rho}+\delta_{\gamma\rho}e_{3\alpha\beta})\varepsilon_{\alpha\beta}\varepsilon_{\gamma\rho}=2A\varepsilon_{\rho\rho}(e_{3\alpha\beta}\varepsilon_{\alpha\beta}) \tag{14}$$

the spherical strain $\varepsilon_{\rho\rho}$ represents the bulk deformation at a material point, it is obviously independent of the handedness of the frame. On the other hand, $e_{3\alpha\beta}\varepsilon_{\alpha\beta}=-2(\phi_3-\psi_3)$is the *pure* rotation of a point, with $\psi_3=e_{3\alpha\beta}u_{\beta,\alpha}/2$ denoting the macro rigid rotation, therefore, it is an axial quantity depending on the handedness. This chiral term in the energy density clearly demonstrates that a pure rotation can produce shrink or dilatation of the material, and vice versa. This mechanism derived from a continuum formulation correctly explains the behavior of a real 2D chiral structure (e.g., the triangular chiral lattice schematically depicted in Fig. 1), which will be discussed in detail in the following section. This can also provide the explanation of the unique mechanism of the chiral lattice to have the negative Poisson's ratio.

The constitutive law of Eq. (13) can be rearranged in a matrix form as

$$\begin{Bmatrix}\sigma_{11}\\ \sigma_{22}\\ \sigma_{12}\\ \sigma_{21}\\ m_{13}\\ m_{23}\end{Bmatrix}=\begin{bmatrix}2\mu+\lambda & \lambda & -A & A & 0 & 0\\ \lambda & 2\mu+\lambda & -A & A & 0 & 0\\ -A & -A & \mu+\kappa & \mu-\kappa & 0 & 0\\ A & A & \mu-\kappa & \mu+\kappa & 0 & 0\\ 0 & 0 & 0 & 0 & \gamma & 0\\ 0 & 0 & 0 & 0 & 0 & \gamma\end{bmatrix}\begin{Bmatrix}u_{1,1}\\ u_{2,2}\\ u_{2,1}-\phi\\ u_{1,2}+\phi\\ \phi_1\\ \phi_2\end{Bmatrix} \tag{15}$$

It has four classical micropolar elastic constants and a new parameter A characterizing the chiral effect. When the handedness of the material pattern is flipped over, the chiral constant A should reverse its sign to maintain the invariance of the strain energy density, and the other constants remain unchanged:

$$\begin{Bmatrix}\sigma_{11}\\ \sigma_{22}\\ \sigma_{12}\\ \sigma_{21}\\ m_{13}\\ m_{23}\end{Bmatrix}=\begin{bmatrix}2\mu+\lambda & \lambda & A & -A & 0 & 0\\ \lambda & 2\mu+\lambda & A & -A & 0 & 0\\ A & A & \mu+\kappa & \mu-\kappa & 0 & 0\\ -A & -A & \mu-\kappa & \mu+\kappa & 0 & 0\\ 0 & 0 & 0 & 0 & \gamma & 0\\ 0 & 0 & 0 & 0 & 0 & \gamma\end{bmatrix}\begin{Bmatrix}u_{1,1}\\ u_{2,2}\\ u_{2,1}-\phi\\ u_{1,2}+\phi\\ \phi_1\\ \phi_2\end{Bmatrix} \tag{16}$$

Finally, with the proposed constitutive equation, the governing equations expressed in the displacements u, v and the microrotation $\phi\equiv\phi_3$ read

$$\rho\frac{\partial^2 u}{\partial t^2}=(\lambda+2\mu)u_{xx}+(\mu+\kappa)u_{yy}+(\lambda+\mu-\kappa)v_{xy}+2\kappa\phi_y-A(v_{xx}-v_{yy}-2u_{xy}-2\phi_x) \tag{17a}$$

$$\rho\frac{\partial^2 v}{\partial t^2}=(\mu+\kappa)v_{xx}+(\lambda+2\mu)v_{yy}+(\lambda+\mu-\kappa)u_{xy}-2\kappa\phi_x-A(u_{xx}-u_{yy}+2v_{xy}-2\phi_y) \tag{17b}$$

$$j\frac{\partial^2 \phi}{\partial t^2}=\gamma(\phi_{xx}+\phi_{yy})-4\kappa\phi+2\kappa(v_x-u_y)-2A(u_x+v_y) \tag{17c}$$

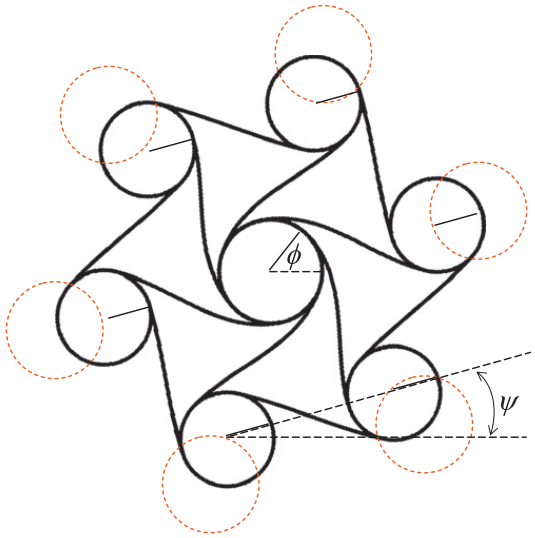

Fig. 1. Visualization of the physical meaning of the 2D chiral micropolar constitutive equation.

The form of Eqs. (15–17) looks like those of an anisotropic medium, however, they are fundamentally different and cannot be recovered by even the most general anisotropy without chirality, since the parameter A and its sign form a unique pattern in the constitutive matrix. They are indeed in-plane isotropic guaranteed by Eq. (12). It should be mentioned that, for the 2D isotropic micropolar solid, Eq. (12) is the only possible form to include chirality.

The constraint conditions on the five material constants can be obtained by imposing positive definiteness of the strain energy density w. It is convenient to decompose the strain tensor into hydrostatic, deviatoric symmetric and antisymmetric parts as (Liu and Hu, 2005)

$$\varepsilon_{\alpha\beta}=\delta_{\alpha\beta}\bar{\varepsilon}+\varepsilon^{d}_{(\alpha\beta)}+\varepsilon_{\langle\alpha\beta\rangle} \tag{18}$$

where

$$\bar{\varepsilon}=\tfrac{1}{2}\varepsilon_{\alpha\alpha} \tag{19a}$$

$$\varepsilon^{d}_{(\alpha\beta)}=\tfrac{1}{2}(\varepsilon_{\alpha\beta}+\varepsilon_{\beta\alpha})-\delta_{\alpha\beta}\bar{\varepsilon} \tag{19b}$$

$$\varepsilon_{\langle\alpha\beta\rangle}=\tfrac{1}{2}(\varepsilon_{\alpha\beta}-\varepsilon_{\beta\alpha})=e_{\beta\alpha3}(\phi-\psi) \tag{19c}$$

Substituting Eqs. (18) and (12) into Eq. (11) yields

$$w=2\bar{\kappa}\,\bar{\varepsilon}^2+2\mu\varepsilon^{d}_{(\alpha\beta)}\varepsilon^{d}_{(\alpha\beta)}+2\kappa(\phi-\psi)^2+4A\bar{\varepsilon}(\phi-\psi)+\tfrac{1}{2}\gamma\phi_{,\alpha}\phi_{,\alpha} \tag{20}$$

where $\bar{\kappa}=\lambda+\mu$ is defined as the 2D bulk (area) modulus. This equation yields the necessary and sufficient conditions for the positive definiteness of w. Besides the four conditions for a classical micropolar medium given in the literature

$$\bar{\kappa}=\lambda+\mu>0,\quad \mu>0,\quad \kappa>0,\quad \gamma>0 \tag{21}$$

an additional condition

$$A^2<(\lambda+\mu)\kappa \tag{22}$$

is imposed on the chiral constant A. It can be either positive or negative, but its absolute value is bounded.

3. Homogenization for a 2D triangular chiral lattice

In this section, we will examine a 2D triangular chiral lattice, and analytically derive the five material constants proposed in the Section 2 by a homogenization method.

3.1. Description of geometry

The geometry of the chiral lattice is shown in Fig. 2. The structural layout consists of circles of radius r linked by straight ligaments of equal length L. The ligaments are required to be tangential to the circles and the angle between adjacent ligaments is $\pi/3$. The circles are arranged as a triangular lattice with the lattice constant, i.e. the distance between circle centers, a. The angle between the line connecting the circle centers and the ligament is defined as β. The geometry parameters are connected by the following relations:

$$\cos\beta=\frac{L}{a},\quad \sin\beta=\frac{2r}{a} \tag{23}$$

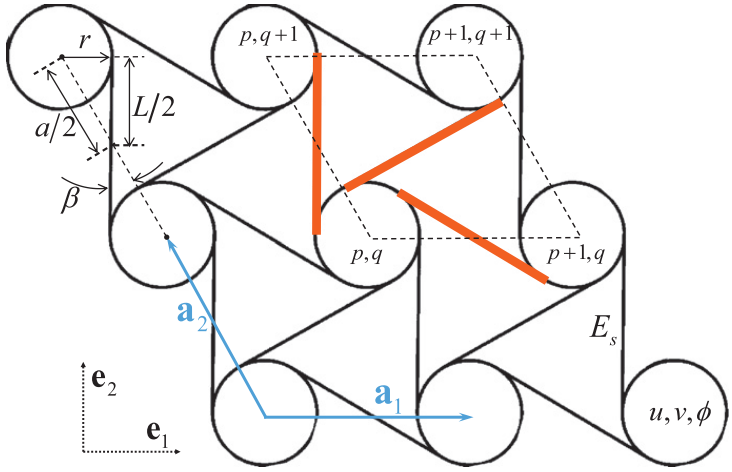

Fig. 2. Geometry of auxectic triangular chiral lattice.

A quadrilateral unit cell is used for the analytical development, as bounded by the dashed parallelogram in Fig. 2. The tessellation of the unit cell along the lattice vectors

$$\mathbf{a}_1 = a\mathbf{e}_x$$
$$\mathbf{a}_2 = -\frac{1}{2}a\mathbf{e}_x + \frac{\sqrt{3}}{2}a\mathbf{e}_y \tag{24}$$

generates the whole lattice. The wall thicknesses of the circles and the ligaments are denoted as t_c and t_b, respectively.

Among the parameters, β is denoted as a topology parameter (Prall and Lakes, 1996; Spadoni et al., 2009). When $\beta \to 0$, the circles shrink to dots and a traditional triangular lattice is obtained. When $\beta \to \pi/2$ the ligaments vanish and a lattice of packed circles is recovered. It should be noted that the chiral effect disappears in these two extreme cases. The parameter β affects not only the topology but also the mechanical behavior of the lattice. As pointed by Spadoni and Ruzzene (2012), the variation of β monitors the transition from bending dominated behavior to axially dominated behavior.

Finally, as shown in Fig. 3, we adopt the sign convention of β according to the relative orientation of the ligament and the link of circle centers. When β reverses its sign, the lattice is flipped over and a complementary pattern with a reversed handedness is implied. This operation cannot be achieved by an in-plane rotation due to its chiral nature.

3.2. Determination of constitutive constants

To formulate the problem analytically, the circles of the chiral lattice are assumed to be rigid. Further, the ligament is assumed to be massless, and the mass and rotation inertia of the rigid circle are denoted as m and J, respectively. However, a numerical procedure (Spadoni and Ruzzene, 2012) can be utilized to deal with the case of deformable circles and distributed mass density.

Let $u_{p,q} = \left\{ u_{p,q} \quad v_{p,q} \quad \phi_{p,q} \right\}^T$ denote the motion of the center of the rigid circle labeled as (p,q), where $u_{p,q}$, $v_{p,q}$ and $\phi_{p,q}$ are the displacement and rotation DOFs, respectively. Referring to Fig. 2, the deformation energy of a quadrilateral unit cell labeled as (p,q) is just contributed from the three deformable ligament beams, and can be determined by the motion of the four related rigid circles as

$$w_{p,q}^{cell} = w(\mathbf{u}_{p,q}, \mathbf{u}_{p+1,q}, \mathbf{u}_{p,q+1}, \mathbf{u}_{p+1,q+1}) \tag{25}$$

The derivation of $w_{p,q}^{cell}$ can be found in the work of Spadoni and Ruzzene (2012), thus the Hamiltonian of the whole lattice system can be obtained as

$$H = \sum\nolimits_{p,q} \left(w_{p,q}^{cell} + \tfrac{1}{2} m\dot{u}_{p,q}^2 + \tfrac{1}{2} m\dot{v}_{p,q}^2 + \tfrac{1}{2} J\dot{\phi}_{p,q}^2 \right) \tag{26}$$

By using Hamilton's principle, the discrete dynamic governing equations for the circle $\mathbf{u}_{p,q}$ are obtained as

$$\rho A_{cell} \frac{\partial^2 u_{p,q}}{\partial t^2} = -\frac{\partial H}{\partial u_{p,q}} \tag{27a}$$

$$\rho A_{cell} \frac{\partial^2 v_{p,q}}{\partial t^2} = -\frac{\partial H}{\partial v_{p,q}} \tag{27b}$$

$$jA_{cell} \frac{\partial^2 \phi_{p,q}}{\partial t^2} = -\frac{\partial H}{\partial \phi_{p,q}} \tag{27c}$$

where the effective density and micro-inertia are defined as $\rho = m/A_{cell}$, $j = J/A_{cell}$, with $A_{cell} = \sqrt{3}a^2/2$ being the area of the unit cell. The right hand side of Eq. (27) contains DOFs $\mathbf{u}_{p,q}$ and those of its adjacent neighbors $\mathbf{u}_{p\pm1,q\pm1}$. The detailed expansion of Eq. (27) is straightforward and will not be presented here.

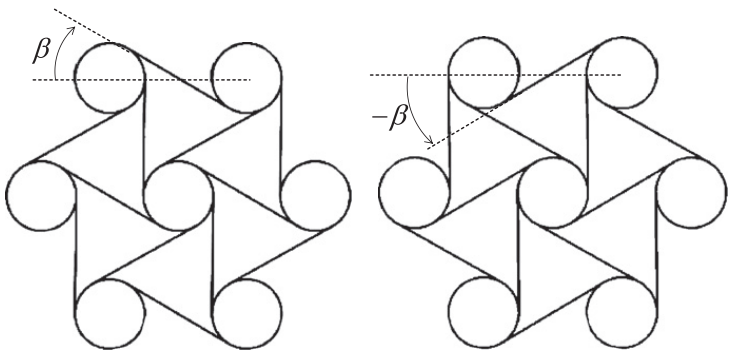

Fig. 3. Chiral lattice with (a) $\beta > 0$ and its handedness reversed pattern with (b) $\beta < 0$.

At long wave limit or the characteristic scale of the problem is much larger than the lattice constant a, the homogenization of the discrete Eq. (27) is possible by representing $u_{p\pm1,q\pm1}$ as its Taylor series expansion at $u_{p,q}$. Specifically, for the displacement u, we have

$$u_{p\pm1,q\pm1}=u+\mathbf{u}'^{T}d\mathbf{x}_{p\pm1,q\pm1}+\tfrac{1}{2}d\mathbf{x}^{T}_{p\pm1,q\pm1}\mathbf{u}''d\mathbf{x}_{p\pm1,q\pm1}+O(|d\mathbf{x}_{p\pm1,q\pm1}|^{2}) \tag{28}$$

where

$$\mathbf{u}'=\left\{\begin{array}{cc}\partial u/\partial x & \partial u/\partial y\end{array}\right\}^{T} \tag{29a}$$

$$\mathbf{u}''=\begin{pmatrix}\partial^2 u/\partial x^2 & \partial^2 u/\partial x\partial y\\ \partial^2 u/\partial x\partial y & \partial^2 u/\partial y^2\end{pmatrix} \tag{29b}$$

and from the relative sites of the circles (Fig. 2), the increments of the position vectors are given by

$$d\mathbf{x}_{p\pm1,q}=\left\{\begin{array}{cc}\pm a & 0\end{array}\right\}^{T} \tag{30a}$$

$$d\mathbf{x}_{p,q\pm1}=\left\{\begin{array}{cc}\mp a/2 & \pm\sqrt{3}a/2\end{array}\right\}^{T} \tag{30b}$$

$$d\mathbf{x}_{\pm(p+1,q+1)}=\left\{\begin{array}{cc}\pm a/2 & \pm\sqrt{3}a/2\end{array}\right\}^{T} \tag{30c}$$

Substituting Eq. (28) and the similar expansions for v and ϕ into Eq. (27) and retaining the leading terms of the spatial differentials yield exactly the governing equations derived in the continuous description (Eq. (17)). This is an encouraging result which confirms the proposed chiral constitutive relation based on the continuum formulation. Then by equating the corresponding coefficients, the effective material constants of the equivalent chiral micropolar medium can be easily obtained,

$$\lambda=\frac{\sqrt{3}E_s}{4}\eta(\cos^2\beta-\eta^2)\sec^3\beta\cos2\beta \tag{31a}$$

$$\mu=\frac{\sqrt{3}E_s}{4}\eta(\cos^2\beta+\eta^2)\sec^3\beta \tag{31b}$$

$$\kappa=\frac{\sqrt{3}E_s}{2}\eta(\sin^2\beta+\eta^2)\sec\beta \tag{31c}$$

$$\gamma=-\frac{E_s a^2}{4\sqrt{3}}\eta\left(3\sin^2\beta+2\eta^2\right)\sec\beta \tag{31d}$$

$$A=\frac{\sqrt{3}E_s}{2}\eta(\eta^2-\cos^2\beta)\sec\beta\tan\beta \tag{31e}$$

where $E_s=E_b/(1-\nu_b{}^2)$ or E_b under a plane strain or plane stress assumption, respectively, with E_b and ν_b being the Young's modulus and Poisson's ratio of the underlying lattice material. Note that in Eq. (31) the slenderness ratio

$$\eta=t/a \tag{32}$$

is defined as the ratio of the ligament wall thickness ($t\equiv t_b$) to the lattice constant.

It can be verified from Eq. (31) that when the chiral lattice is flipped over (sign of β is reversed), A changes its sign, while all the other parameter remains unchanged, which is just the same as that predicted by Eq. (15) and (16). When $\beta=0$ for a traditional triangular lattice, A vanishes and the chiral effect disappears, the remaining effective material constants are reduced to

$$\lambda=\frac{\sqrt{3}E_s t}{4a^3}(a^2-t^2) \tag{33a}$$

$$\mu=\frac{\sqrt{3}E_s t}{4a^3}(a^2+t^2) \tag{33b}$$

$$\kappa=\frac{\sqrt{3}E_s t^3}{2a^3} \tag{33c}$$

$$\gamma=-\frac{E_s t^3}{2\sqrt{3}a} \tag{33d}$$

which are the same as those given by Kumar and McDowell (2004) for a triangular lattice by considering up to the second order expansion of the microrotation DOF. With this homogenization scheme, the obtained higher order modulus γ for the

lattice structures is always negative, since the microrotation on the unit cell is approximated by a second order Taylor's expansion (Bazant and Christensen, 1972; Kumar and McDowell, 2004). However, the first order method (Chen et al., 1998; Kumar and McDowell, 2004; Spadoni and Ruzzene, 2012), i.e. retaining the first order items of Eq. (38) and by using the equivalence of the unit cell energy density $w_{p,q}^{cell}/A_{cell}$ with the continuum medium, Eq. (11), is also examined, and a positive version of the higher order modulus is obtained as

$$\gamma = \frac{E_s a^2}{4\sqrt{3}}\eta\left(3\sin^2\beta + 4\eta^2\right)\sec\beta \tag{34}$$

with the other effective material constants in Eq. (31) remaining unchanged. It also reduces to the results considering only the first order expansion when $\beta=0$ (Chen et al., 1998; Kumar and McDowell, 2004). The negative or positive values of gamma depend on the selection of retaining or not the second order derivatives of the microrotation in the energy expression of the unit cell. From the viewpoint of the equilibrium of lattice joint, gamma should be negative (Bazant and Christensen, 1972), on the other hand, it should be positive regarding to the positive definiteness of strain energy (Eringen,1966). Kumar and McDowell (2004) provided an insightful explanation for this contradiction and reference computations on the two versions of the higher order modulus γ. Basically, negative γ is not suitable in the static problem since the terms like $e^{\sqrt{\gamma}}$ appears in the solution, which results in a nonphysical fluctuant mechanical field (Kumar and McDowell, 2004).

If the lattice with deformable node circles is considered, numerical homogenization procedure based on the unit cell finite element calculation can be employed. We found that the chiral effect of the lattice is also pronounced in case of deformable circles, which is in accordance with the main conclusion with the rigid ring. The details of the case with deformable node circles can be found in the supplementary material.

4. Discussions and applications

In this section, we will discuss in detail the obtained effective material constants for the triangular chiral lattice. A static tension problem and a plane wave analysis will also be examined in order to illustrate the proposed theory.

4.1. Properties of the effective material constants

First, we will compare the derived effective material constants in Eq. (31) with those derived from a non-chiral micropolar theory (see Eqs. (25–34) in Spadoni and Ruzzene (2012)) for the same chiral lattice. In the following, λ_a, μ_a, κ_a and γ_a are denoted as the non-chiral version of the effective constants.

Comparing the results predicted by the chiral and non-chiral theories, it is found that the two theories give the same prediction on the modulus μ and κ as well as the higher order modulus γ, but different on λ. Of course the parameter A is only introduced in the current chiral theory. In Fig. 4, A, λ and λ_a normalized y E_s are plotted as function of β, where

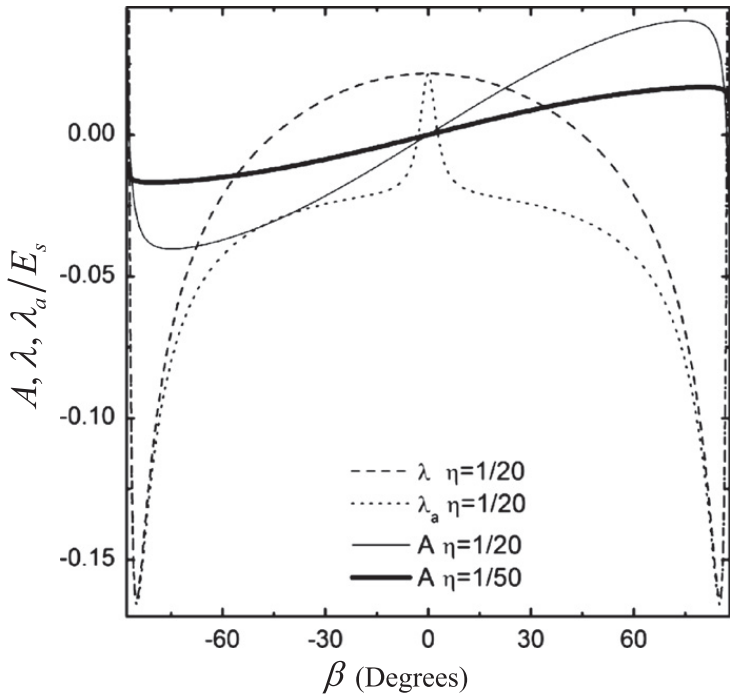

Fig. 4. Effective Lame constant λ predicted by chiral and non-chiral theory, and the effective chiral constant with different microstructure parameters.

$\eta=1/20$ is used in the calculation. It is shown that the chiral constant is an odd function of β and $|A|$ increases with the increase of $|\beta|$ in the region of roughly $|\beta|<75^\circ$, this indicates that the bulk-rotation coupling behavior becomes stronger with the increase of circle size. It should also be noted here that since the beam theory is used the results may not be accurate or even meaningless for $\beta\to 90^\circ$, where the ligament is vanishingly short. An additional curve is also included in the figure for the parameter A with a slenderness $\eta=1/50$, the result shows that the chiral constant also increases for greater ligament width. Physically positive A means, regarding to the constitutive Eq. (15), an anticlockwise circle rotation, which will induce a hydrostatic compression, while all the other strain components are hold to be zero. This is just the case for the lattice shown in Fig. 3a. The scenario should be reversed for another handedness, Fig. 3b. Finally, from Eq. (31), we get

$$(\lambda+\mu)\kappa-A^2=\tfrac{3}{4}(\eta\sec\beta)^4\geq 0 \tag{35}$$

which confirms that the thermodynamic stability requirement on the chiral constant, Eq. (22), is always fulfilled.

An unusual characteristic of the non-chiral micropolar (and also the classical elasticity since they are the same in bulk behavior) homogenization of the chiral lattice is the negativity of λ. This is obvious since the chiral lattice produces negative Poisson's ratio $\nu=\lambda/(\lambda+2\mu)$. However, Fig. 4 shows that the current chiral homogenization gives significant variation of λ, thus it seems that the effective Poisson's ratio would be no longer negative in some ranges of the parameter β. Based on the constitutive Eqs. (15) and (16), the Poisson's ratio of a chiral micropolar medium must be redefined. By defining $\nu=-\varepsilon_{22}/\varepsilon_{11}$ and assuming all the stress components except for σ_{11} are zero, we have

$$\lambda\varepsilon_{11}+(\lambda+2\mu)\varepsilon_{22}-A(\varepsilon_{12}-\varepsilon_{21})=0 \tag{36a}$$

$$-A(\varepsilon_{11}+\varepsilon_{22})+(\mu+\kappa)\varepsilon_{12}+(\mu-\kappa)\varepsilon_{21}=0 \tag{36b}$$

$$A(\varepsilon_{11}+\varepsilon_{22})+(\mu-\kappa)\varepsilon_{12}+(\mu+\kappa)\varepsilon_{21}=0 \tag{36c}$$

Solving the above equations gives the Poisson's ratio for the chiral micropolar medium

$$\nu=\frac{\lambda-A^2/\kappa}{\lambda+2\mu-A^2/\kappa} \tag{37}$$

The sign of the chiral constant does not affect the Poisson's ratio. Physically this means the auxetic behavior is independent of the direction of internal rotation of the circles, as expected. The Young's modulus now becomes

$$E=\frac{(\lambda+2\mu-A^2/\kappa)^2-(\lambda-A^2/\kappa)^2}{\lambda+2\mu-A^2/\kappa} \tag{38}$$

By using Eq. (31), the overall Young's modulus and Poisson's ratio of the chiral lattice are explicitly expressed as

$$\nu=\frac{1-\eta^2-(\cos\beta\sin\beta/\eta)^2}{3+\eta^2+(\cos\beta\sin\beta/\eta)^2} \tag{39}$$

$$E=2\sqrt{3}E_s\eta^3\frac{\sec^3\beta[\eta^2+\cos^2\beta]}{3\eta^2+\eta^4/8+\cos^2\beta\sin^2\beta} \tag{40}$$

From Eq. (39), $\nu\approx 1/3$ (slightly affected by the ligament slenderness) for the two extreme values of β, while for the other geometry $\nu\approx -1$since the $1/\eta$ term dominates. In fact, it is interesting to verify that the above expressions are exactly the same as the non-chiral prediction by Spadoni and Ruzzene (2012). The other commonly used parameters such as the characteristic length $l^2=\gamma/\mu$ and the coupling number $N^2=\kappa/(\kappa+\mu)$ (Cowin, 1970) are also the same as those derived from the non-chiral theory. In summary, the proposed chiral micropolar theory introduces the chiral parameter A to capture the coupling between the bulk deformation and the internal rotation, and is only different in the prediction on Lame's constant λ compared with the non-chiral micropolar theory.

4.2. One dimensional static tension

We consider in the following a one dimensional tension problem of the chiral micropolar medium, as shown in Fig. 5a. A sourceless domain is l in size in x direction, and infinite in y direction. A constant displacement u^o is prescribed on the right side while all the other DOFs are fixed on the boundary. Since the problem is infinite in y direction, the field quantities are only the functions of x, the strains are then $\varepsilon_{xx}=u'$, $\varepsilon_{yy}=0$, $\varepsilon_{xy}=v'-\phi$ and $\varepsilon_{yx}=\phi$, where a prime means the ordinary differential with respect to x. With the help of the constitutive and equilibrium equations, we obtain

$$(\lambda+2\mu)u''-Av''+2A\phi'=0 \tag{41a}$$

$$-Au''+(\mu+\kappa)v''-2\kappa\,\phi'=0 \tag{41b}$$

$$\gamma\,\phi''-4\kappa\,\phi+2\kappa v'-2Au'=0 \tag{41c}$$

with the boundary conditions shown in Fig. 5a.

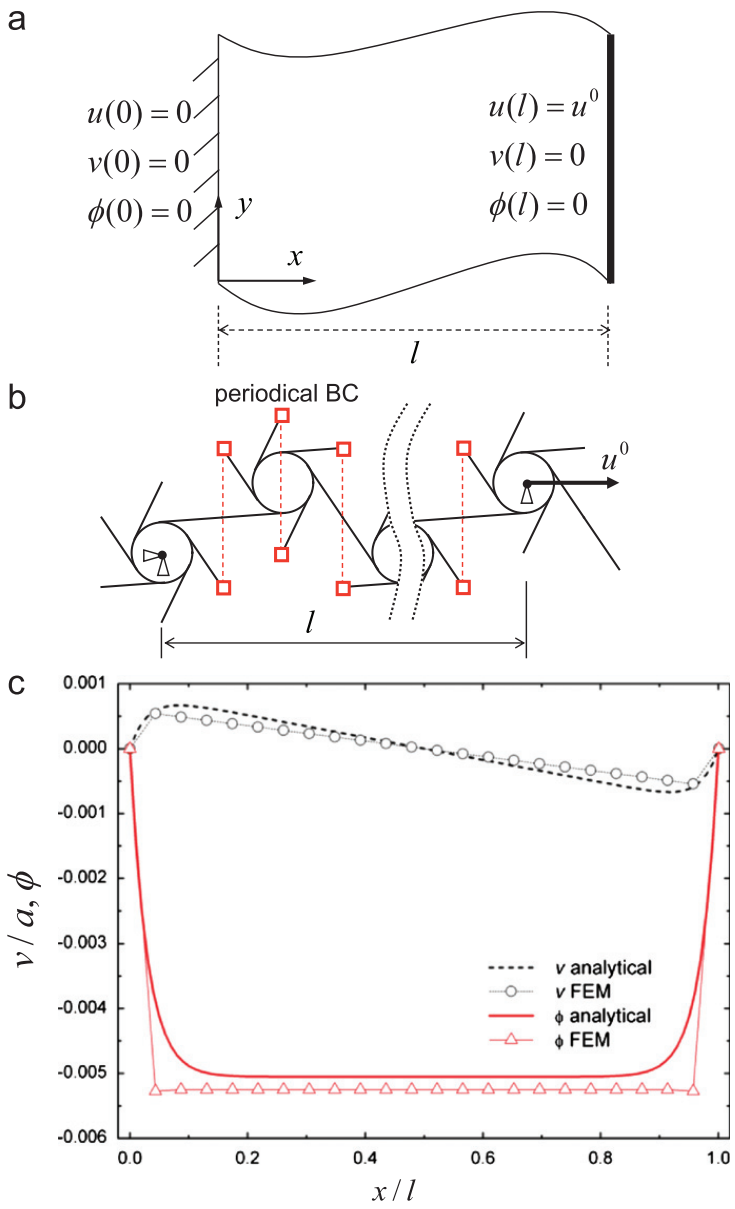

Fig. 5. (a) Problem definition and (b) sketch of corresponding discrete FEM model for the one-dimensional tension; (c) lateral displacement and microrotation fields.

For the classical micropolar case ($A=0$), the solution is identical with that by the Cauchy elasticity, since Eq. (41a) is decoupled from the other two and forms a complete boundary value problem, while v and ϕ are zero conforming the homogeneous boundary conditions. When the chirality appears, the variables in Eq. (41) are coupled together, this implies that even a simple tension in x direction will produce the displacement in y direction, as well as the rotational field. This basic behavior cannot be predicted with the existing 2D version of the non-centrosymmetric micropolar theory.

As an example, Eq. (41) is solved with the parameters $l=20a$, $\eta=1/20$, and $u^o=a/10$. A discrete model of the finite element method (FEM) is constructed with the same parameters as sketched in Fig. 5b. The rigid circle is modeled by the constraint equations which connect the six nodes on the circle to the nodes at its center. The infinite size in y direction is mimicked by periodic boundary conditions with the matched nodes on each side, and the same boundary conditions as Fig. 5a are point-wisely enforced. As mentioned in the previous section, the negative version of high-order modulus γ causes non-physical fluctuation in static solution, the positive version of Eq. (34) is used in this problem. The displacement v and the microrotation ϕ predicted by the analytical and FEM solutions are displayed in Fig. 5c, a fairly good agreement is found between the two methods. Due to the chirality of the lattice structure, the displacement in y increases in an asymmetrical manner in the vicinity of the boundary, and soon becomes affine across the x length, which creates an inclined deformed sample. It is also found that the significant variation portion of the fields near the boundary is nearly independent of the length l, this can be attributed to the boundary layer effect (Eringen, 1999) and agrees with the traditional micropolar theory. If the handedness of the microstructure of the FEM model is changed, i.e., the model is mirror reflected with respect to x axis, the field distribution should be also reflected. For the analytical model, this is a

natural result by inversing the sign of the chiral constant ($-A$). The non-chiral micropolar theory always gives trivial solutions for v and ϕ. Though the displacement in y caused by the tension in x is relatively small for the static case, such effect would become more pronounced for wave propagation, as demonstrated in the following section.

4.3. Plane wave propagation

Considering in an infinite planar chiral micropolar medium under a plane wave in $+x$ direction, the displacement and the microrotation are assumed to be the following from

$$(u,v,\phi)=(\hat{u},\hat{v},\hat{\phi})\exp(ikx-i\omega t) \tag{42}$$

where k and ω denote the wave number and circular frequency, $(\hat{u},\hat{v},\hat{\phi})$ are the (complex) amplitudes, and $i=\sqrt{-1}$. Substituting Eq. (42) into Eq. (17) yields the following secular equation system for the chiral micropolar medium:

$$\begin{pmatrix} k^2(\lambda+2\mu)-\omega^2\rho & -Ak^2 & -2iAk \\ -Ak^2 & k^2(\kappa+\mu)-\omega^2\rho & 2i\kappa k \\ 2iAk & -2ik\kappa & (k^2\gamma+4\kappa)-\omega^2 j \end{pmatrix}\begin{pmatrix}\hat{u}\\ \hat{v}\\ \hat{\phi}\end{pmatrix}=0 \tag{43}$$

Let $A=0$, we obtain the secular equation for a classical micropolar medium without chirality

$$\begin{pmatrix} k^2(\lambda+2\mu)-\omega^2\rho & 0 & 0 \\ 0 & k^2(\kappa+\mu)-\omega^2\rho & 2i\kappa k \\ 0 & -2ik\kappa & (k^2\gamma+4\kappa)-\omega^2 j \end{pmatrix}\begin{pmatrix}\hat{u}\\ \hat{v}\\ \hat{\phi}\end{pmatrix}=0 \tag{44}$$

The most pronounced difference between the chiral and non-chiral micropolar media is that for the later one a non-dispersive longitudinal wave with velocity $c_p=\sqrt{(\lambda+2\mu)/\rho}$ can always be decoupled from the other two shear-rotation coupled waves (Eringen, 1999). This is the characteristic of the non-chiral micropolar media, i.e. the microrotation is only coupled with shear but not with dilatation. In the current chiral micropolar theory, as implied by Eqs. (11–13), the rotation is coupled with the dilation deformation due to the non-zero chiral constant A. Hence there would be no longer pure P or pure S wave in such media. The three wave modes are all mixed and dispersive, thus we call P, S or R (rotation) dominated waves, respectively. Since the full matrix in Eq. (43) will result in a full third order equation, the analytical eigen-solution is tedious, we will instead numerically evaluate it through examples.

The wave behavior in an isotropic 3D chiral micropolar medium has been addressed in the literature (Lakhtakia et al., 1988; Ro, 1999; Khurana and Tomar, 2009). A remarkable feature is that the transverse (shear and rotation coupled) waves can be distinguished as left circular polarized (LCP) and right circular polarized (RCP) waves, which means that the ratio of the two displacement (also the rotation) components equals to $\pm i$ and not in the same phase. The LCP and RCP waves propagate at different phase speeds, this reveals the lack of mirror symmetry of the underlying chiral microstructure inherent in the material. From Eq. (43), it is easy to obtain the ratio of the two displacement amplitudes as

$$\frac{\hat{u}}{\hat{v}}=\frac{k^2[A^2-\kappa(\lambda+2\mu)]+\kappa\omega^2\rho}{Ak^2\mu-\omega^2\rho)} \tag{45}$$

Obviously this ratio cannot be an imaginary number, therefore the common feature (circular polarization) for 3D chiral micropolar media is not presented in the 2D version, and the particle motion under the wave is always linearly polarized. However, the loss of mirror symmetry is reflected in another way for the 2D case. Because the medium is in-plane isotropic, the frequency dispersion must be isotropic and independent of the propagating direction, i.e. the iso-frequency contour of this medium should be concentric circles. On the other hand, the displacement polarization will remain the same angle with respect to the wave vector. This result is schematically shown in Fig. 6a. The polarization according to the wave vector $\boldsymbol{k}$ forms a pattern with a rotational symmetry, but without mirror reflective symmetry. It is interesting to note that the P- and S-mixed wave modes can be traditionally observed in the anisotropic medium, but we can find the mixed wave modes in a 2D chiral micropolar medium while the dispersion is isotropic. This wave phenomenon is not reported before.

In the following, numerical solutions based on the chiral and non-chiral micropolar theories for the same chiral lattice will be conducted. For comparison, the exact dispersive solution of the chiral lattice is also calculated from the Bloch wave (Brillouin, 1953) solution of the discrete kinetic Eq. (27), by adopting the following lattice wave function

$$(u,v,\phi)_{p,q}=(\hat{u},\hat{v},\hat{\phi})_{p,q}\exp(ikx_{p,q}-i\omega t) \tag{46}$$

where the location of certain rigid circle $x_{p,q}$ takes the similar value as Eq. (30). The wave frequency$\omega$is normalized by

$$\Omega=\sqrt{\frac{4E_s t^3}{ma^3}} \tag{47}$$

which represents the natural frequency of a simple supported beam with a lumped mass at its middle. Parameters $\beta=0.9$, $\eta=1/20$, $m=J=1$ are used in the numerical example.

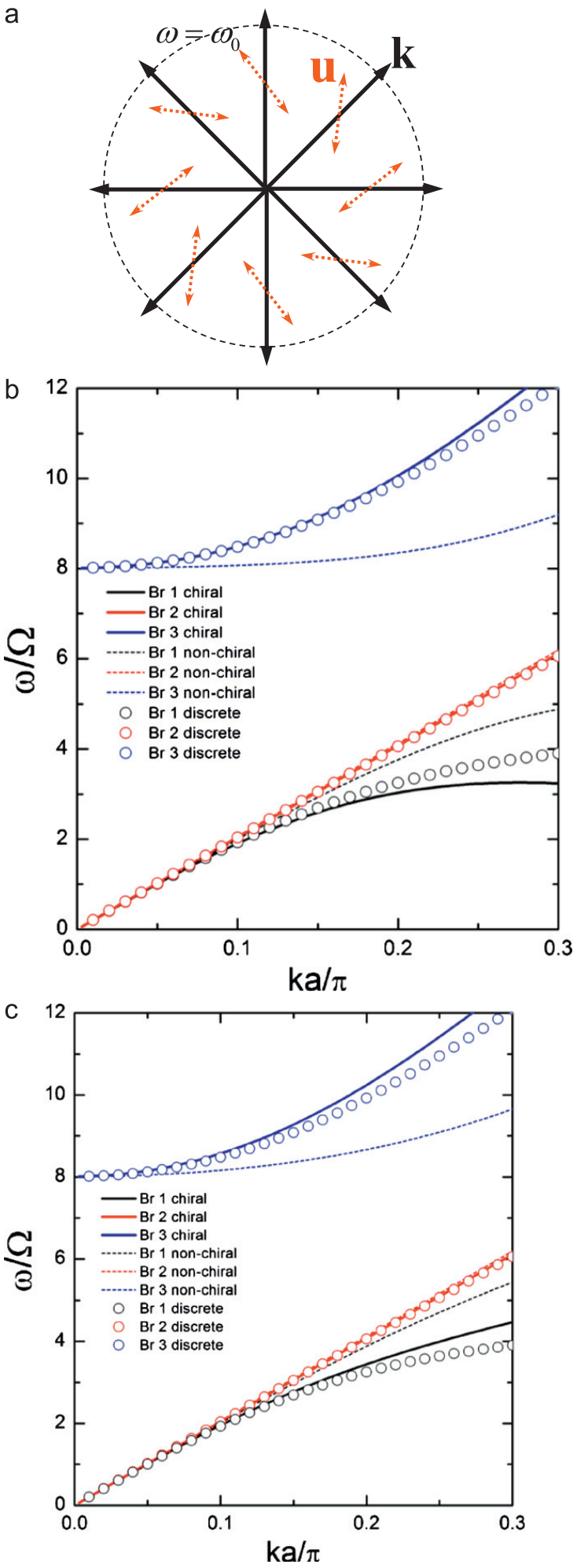

Fig. 6. (a) Schematic wave behavior of the 2D chiral media; Comparison dispersion relations for the chiral, non-chiral homogenization employing negative (b) and positive (c) versions of higher order modulus, with the discrete model. (For interpretation of the references to color in this figure, the reader is referred to the web version of this article.)

Fig. 6b shows the three branches (in black, red and blue, respectively) of the dispersion curves, predicted by the chiral micropolar theory (solid line), the non-chiral micropolar theory (dashed line) and the discrete model (circles), respectively. The first and second branches correspond to the displacement dominated modes and the third one is the rotational dominated wave. The second branch is almost non-dispersive. For the non-chiral theory this is just the uncoupled non-dispersive P-wave, while they are slightly dispersive predicted by both the chiral theory and discrete model. All three models agree well for this branch. However, for the first and third branches, the chiral theory agrees well with those given by the discrete model and a large discrepancy between the chiral and the non-chiral micropolar theory is found. It is also interesting to notice that the dispersion curves of P and S dominated waves almost coincide at the long wave limit, indicating almost same phase wave velocities. This is the feature of waves in materials with Poisson's ratio $\nu \approx -1$, where the shear modulus is much greater than the bulk modulus (Spadoni and Ruzzene, 2012).

In the Fig. 6b, the negative value of the high-order modulus γ in Eq. (31d) is used. For a comparison, the dispersion relation using the positive one, Eq. (34), is also shown by Fig. 6c. It is seen that the results of these two versions differ only slightly, particularly for the second branch. However, no matter positive or negative γ values are employed, the chiral theory predicts consistently better results than the non-chiral theory.

To further examine the wave modes, here we focus on the displacement dominated one, i.e., the first and second branches. Since the particle is linearly polarized, it is convenient to define a polarization angle Λ with respect to the wave propagating direction, i.e., in x direction

$$\tan\Lambda = |\hat{v}/\hat{u}| \tag{48}$$

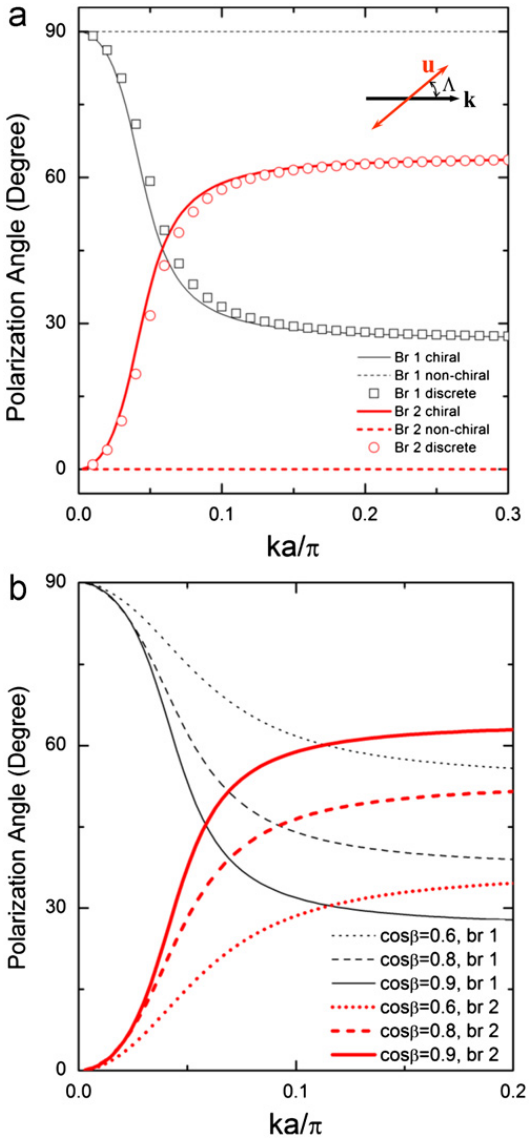

Fig. 7. (a) Comparison of the polarization angle for the chiral, non-chiral homogenization and the discrete model; (b) Polarization variation for the first two branches with different topology parameters. (For interpretation of the references to color in this figure, the reader is referred to the web version of this article.)

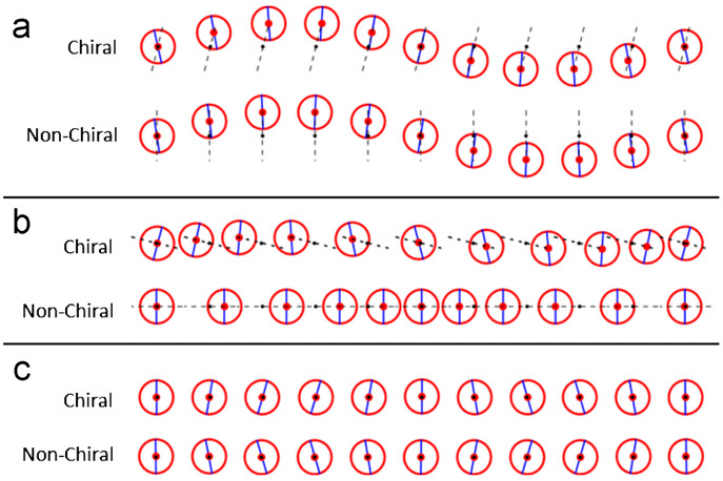

Fig. 8. Wave shapes compared with non-chiral micropolar theory: (a) S-dominated; (b) P-dominated; and (c) rotational dominated.

The polarization angle of the two waves predicted by the chiral and non-chiral theories are plotted in Fig. 7a as function of the wave number, where the first and second branches are marked in black and red, respectively. The non-chiral theory always predicts pure P- and S-waves, thus the polarization angles remain to be 0° and 90°, as expected. For the chiral theory, the S and P dominated wave (for example $\Lambda > 60^\circ$and $\Lambda < 30^\circ$) can be observed when the wave number is small ($ka < 0.05$) for the first and second branches, respectively. However, for the intermediate wave number ($ka > 0.05$), the first two branches become indistinguishable and can even interchange, i.e. the first branch become P dominated and the second branch become S dominated. Again, the predictions by the proposed chiral micropolar model always agree well with those by the discrete model (shown by circle and square dots). Polarizations corresponding to different topology parameters are also shown in Fig. 7b. It is found that the P- and S- wave modes will be more mixed for larger $\cos\beta$, i.e., smaller circles for the same lattice constant.

For further illustrating the unique wave behavior of the proposed theory, snapshots of wave modes of the three branches are shown in Fig. 8 according to the solutions of Eqs. (42) and (43), where the wave number $k=0.03\pi/a$ is used. The wave modes are shown in 10 material particles represented by circles in a period, whereas a short line in the particle identifies its rotation. The particle trajectory, i.e. the polarization direction, is highlighted by the dashed line. For the first branch shown in Fig. 8a, particle translation and rotation are found for both the chiral and non-chiral theories. However, the polarization is purely transverse for the non-chiral theory, while it is transverse dominated for the current chiral theory. For the second branch shown in Fig. 8b, a pure longitudinal wave without particle rotation is predicted for the non-chiral theory, while for the chiral theory it is longitudinal dominated with particle rotation. For the third branch shown in Fig. 8c, the particle translations are small in both cases, hence only particle rotations almost at their original sites are observed.

5. Conclusions

The existing micropolar theory is not able to characterize the chiral effect inherent in plane isotropic chiral solids, e.g. triangle chiral lattices. In the paper, we propose a continuum theory to capture the chiral effect in such materials. The proposed method is based on the micropolar theory and reinterpretation of in-plane isotropic tensors. The constitutive equation and the governing equation are analytically derived. Different from the existing 2D isotropic micropolar theory, a new material constant is introduced to characterize the chiral effect, it can be either positive or negative depending on the handedness of the material while its absolute value is bounded. Physically, the proposed chiral micropolar theory can describe the dilatation–rotation coupling, in addition to the conventional shear–rotation coupling.

Based on the theory, we also propose a homogenization scheme for a triangle chiral lattice, from which the effective material parameters of the chiral lattice are derived analytically. By introducing the new material parameter, the proposed homogenization method gives different prediction on the Lames constant λ, but the other effective material constants remain the same as those predicted by the non-chiral version. The problems of the triangle chiral lattice under a static tension and a plane wave loading conditions are examined. For the static tension loading, it is found that even a simple tension can induce rotation and lateral displacement fields inside of the material, as expected. For the plane wave loading, there is no longer pure longitudinal and transverse waves, and all the wave modes are of mixed types and dispersive. Mixed wave modes with isotropic frequency dispersion are also observed, which is a fundamental property of a planar isotropic chiral solid. This special wave phenomenon is not reported before. These results are finally verified by the exact solution of the corresponding discrete model. Hopefully, the proposed method can provide a useful tool to investigate the chiral effect on mechanical behavior of plane isotropic chiral solids.

Acknowledgment

This work was supported in part by Air Force Office of Scientific Research under Grant no. AF 9550-10-0061 with Program Manager Dr. Byung-Lip (Les) Lee and NSF 1037569, and in part by National Natural Science Foundation of China under Grant nos. 10972036, 10832002 and 11072031, and the National Basic Research Program of China (Grant no. 2011CB610302).

Appendix A. Supporting information

Supplementary data associated with this article can be found in the online version at http://dx.doi.org/10.1016/j.jmps.2012.06.008.

References

Alderson, A., Alderson, K.L., Attard, D., Evans, K.E., Gatt, R., Grima, J.N., Miller, W., Ravirala, N., Smith, C.W., Zied, K., 2010. Elastic constants of 3-, 4- and 6-connected chiral and anti-chiral honeycombs subject to uniaxial in-plane loading. Compos. Sci. Technol. 70, 1042–1048.
Auffray, N., Bouchet, R., Brechet, Y., 2010. Strain gradient elastic homogenization of bi-dimensional cellular media. Int. J. Solids Struct. 47, 1698–1710.
Bazant, Z.P., Christensen, M., 1972. Analogy between micropolar continuum and grid frameworks under initial stress. Int. J. Solids Struct. 8, 327–346.
Borisenko, A.I., Tarapov, I.E., 1979. Vector and Tensor Analysis with Applications. Dover Publications, New York.
Brillouin, L., 1953. Wave Propagation in Periodic Structures. Dover, New York.
Chandraseker, K., Mukherjee, S., 2006. Coupling of extension and twist in single-walled carbon nanotubes. J. Appl. Mech. 73, 315–326.
Chandraseker, K., Mukherjee, S., Paci, J.T., Schatz, G.C., 2009. An atomistic-continuum Cosserat rod model of carbon nanotubes. J. Mech. Phys. Solids 57, 932–958.
Chen, J.Y., Huang, Y., Ortiz, M., 1998. Fracture analysis of cellular materials: a strain gradient model. J. Mech. Phys. Solids 46, 789–828.
Cosserat, E., Cosserat, F., 1909. Théorie des Corps Déformables. A. Hermann, Paris.
Cowin, S.C., 1970. An incorrect inequality in micropolar elasticity theory. Z. Angew. Math. Phys. 21, 494–497.
Dirrenberger, J., Forest, S., Jeulin, D., Colin, C., 2011. Homogenization of periodic auxetic materials. Proc. Eng. 10, 1847–1852.
Eringen, A.C., 1966. Linear theory of micropolar elasticity. J. Math. Mech. 15, 909–923.
Eringen, A.C., 1999. Microcontinuum Field Theories I: Foundations and Solids. Springer, New York.
Ieşan, D., 2010. Chiral effects in uniformly loaded rods. J. Mech. Phys. Solids 58, 1272–1285.
Joumaa, H., Ostoja-Starzewski, M., 2011. Stress and couple-stress invariance in non-centrosymmetric micropolar planar elasticity. Proc. R. Soc. A http://dx.doi.org/10.1098/rspa.2010.0660. (Published online).
Kelvin, Lord, 1904. Baltimore Lectures on Molecular Dynamics and the Wave Theory of Light. C. J. Clay and Sons, London.
Khurana, A., Tomar, S.K., 2009. Longitudinal wave response of a chiral slab interposed between micropolar solid half-spaces. Int. J. Solids Struct. 46, 135–150.
Kumar, R.S., McDowell, D.L., 2004. Generalized continuum modeling of 2-D periodic cellular solids. Int. J. Solids Struct. 41, 7399–7422.
Lakes, R., 2001. Elastic and viscoelastic behavior of chiral materials. Int. J. Mech. Sci. 43, 1579–1589.
Lakes, R., Yoon, H.S., Katz, J.L., 1983. Slow compressional wave propagation in wet human and bovine cortical bone. Science 220, 513–515.
Lakes, R.S., 1987. Foam structures with a negative Poisson's ratio. Science 235, 1038–1040.
Lakes, R.S., Benedict, R.L., 1982. Noncentrosymmetry in micropolar elasticity. Int. J. Eng. Sci. 20, 1161–1167.
Lakhtakia, A., Varadan, V.V., Varadan, V.K., 1988. Elastic wave propagation in noncentrosymmetric, isotropic media: Dispersion and field equations. J. Appl. Phys. 63, 5246–5250.
Liu, X.N., Hu, G.K., 2005. A continuum micromechanical theory of overall plasticity for particulate composites including particle size effect. Int. J. Plast. 21, 777–799.
Liu, X.N., Hu, G.K., Huang, G.L., Sun, C.T., 2011a. An elastic metamaterial with simultaneously negative mass density and bulk modulus. Appl. Phys. Lett. 98, 251907.
Liu, X.N., Hu, G.K., Sun, C.T., Huang, G.L., 2011b. Wave propagation characterization and design of two-dimensional elastic chiral metacomposite. J. Sound Vib. 330, 2536–2553.
Natroshvili, D., Stratis, I.G., 2006. Mathematical problems of the theory of elasticity of chiral materials for Lipschitz domains. Math. Methods Appl. Sci 29, 445–478.
Natroshvili, D., Giorgashvili, L., Stratis, I.G., 2006. Representation formulae of general solutions in the theory of hemitropic elasticity. Q. J. Mech. Appl. Math. 59, 451–474.
Nowacki, W., 1986. In: Theory of Asymmetric ElasticityPergamon Press, New York.
Prall, D., Lakes, R.S., 1996. Properties of a chiral honeycomb with a Poisson's ratio ≈ -1. Int. J. Mech. Sci. 39, 305–314.
Ro, R., 1999. Elastic activity of the chiral medium. J. Appl. Phys. 85, 2508–2513.
Spadoni, A., Ruzzene, M., 2012. Elasto-static micropolar behavior of a chiral auxetic lattice. J. Mech. Phys. Solids 60, 156–171.
Spadoni, A., Ruzzene, M., Gonella, S., Scarpa, F., 2009. Phononic properties of hexagonal chiral lattices. Wave Motion 46, 435–450.
Wang, J.S., Jun, Feng X.Q., Qin, Q.H., Yu, S.W., 2011. Chirality transfer from molecular to morphological scales in quasi-one-dimensional nanomaterials: a continuum model. J. Comput. Theor. Nanosci. 8, 1–10.
Yang, W., Li, Z.M., Shi, W., Xie, B.H., Yang, M.B., 2004. Review on auxetic materials. J. Mater. Sci. 39, 3269–3279.